KFUPM
Journal of Undergraduate Research International

Diamond Open Access 100
Article Geosciences

Diagenetic Alteration of Glauconitic Greensand: Experimental Constraints on Smectite-Rich Phase Formation, Illitization, and Reservoir Quality Evolution

Fatimah Al Ibrahim and Anas Muhammad Salisu*

Cite https://doi.org/10.64589/juri/231548

Submitted: April 26, 2026 **Revised:** May 12, 2026 **Accepted:** May 15, 2026

ABSTRACT

Glauconitic greensands often undergo clay mineral transformations during burial, influencing reservoir properties. Despite their widespread occurrence, the diagenetic pathways governing the alteration of glauconitic greensands remain insufficiently constrained. This study experimentally investigated the progressive diagenetic alteration of glauconite-rich greensand and evaluated its implications on the evolution of reservoir quality. We performed four 21-d batch experiments at 80, 150, 200, and 250 °C, using natural seawater and a Cretaceous glauconitic greensand as starting material. The reaction products were characterized using X-ray diffraction, X-ray fluorescence, scanning electron microscopy, and fluid chemistry analysis. Several distinct alteration stages were observed. At 80 °C, partial dissolution of glauconite and detrital phases enriched the fluid in Mg and K without authigenic clay formation. Smectite first developed at 150 °C as a grain-coating clay. At 200 °C, smectite partially transformed to mixed-layer illite–smectite and was accompanied by increasing aqueous K, indicating rapid dissolution of K-feldspar. At 250 °C, the assemblage was dominated by fibrous illite. These results demonstrate a temperature-dependent transformation pathway from glauconite to smectite, and ultimately to illite. Furthermore, grain-coating clays that formed during the intermediate stages may inhibit quartz cementation and preserve porosity, whereas late-stage fibrous illite can reduce permeability by blocking pore throats. Overall, glauconite-driven clay evolution may preserve the total pore volume while degrading fluid flow, with the net reservoir quality controlled by clay morphology and distribution.

Keywords: glauconite; smectite; illitization; clay diagenesis; reservoir quality; grain-coating clays

1. INTRODUCTION

Glauconitic greensands are widely distributed in marine sedimentary successions and occur as sand- to silt-sized pellets and granules formed at low sedimentation rates with sustained seawater circulation [1,2]. These deposits are common in shelf-to-upper-slope environments and well-documented in many hydrocarbon-producing basins worldwide [3–5]. Owing to their relatively high primary porosity and association with quartz-rich sand bodies, glauconitic sandstones frequently serve as important hydrocarbon reservoirs and are increasingly being considered for subsurface energy applications [1,6]. However, glauconitic greensands do not remain mineralogically static during burial. Progressive diagenetic alteration modifies glauconite and its associated detrital phases through fluid–rock interactions, leading to changes in clay mineral composition and texture, which can substantially influence reservoir quality.

Clay minerals exert strong control over the reservoir quality by modifying both porosity and permeability [7]. The early development of grain-coating clays may inhibit quartz overgrowth and help preserve pore space [8–10], whereas pore-filling or fibrous clays can block pore throats and restrict fluid flow [11]. In many sedimentary systems, smectite forms under relatively low-temperature diagenetic conditions, subsequently transforming into mixed-layer illite–smectite (I/S) and finally illite as the temperature and potassium availability increase [12,13]. This smectite-to-illite transformation is one of the most significant burial reactions in siliciclastic reservoirs, linking clay mineral evolution to the thermal history and fluid chemistry of the associated basin. The morphology, distribution, and composition of these authigenic clays ultimately determine whether reservoir quality is enhanced or degraded during burial.

Although smectite formation and illitization have been widely studied in mudstones and conventional sandstones [14–17], the diagenetic evolution of glauconite-rich greensands remains underexplored. In particular, the pathways, temperature range, and textural consequences of glauconite-to-smectite alteration and its subsequent transformation to illite are not well understood, limiting the prediction of reservoir quality evolution in glauconitic sandstones.

To address this gap, a glauconitic greensand from the Upper Cretaceous Arnager Formation was subjected to controlled

Published under an exclusive license by KFUPM

Table 1. *Experimental conditions*

Experiment	Sample ID	Solution	Duration (weeks)	Temperature (°C)
1	GL@80	Sea Water	3	80
2	GL@150	Sea Water	3	150
3	GL@200	Sea Water	3	200
4	GL@250	Sea Water	3	250

hydrothermal experiments at 80–250 °C using a high fluid-to-rock ratio. The reaction products and fluids were analyzed using integrated petrographic, mineralogical, and geochemical methods to track the temperature-dependent dissolution–precipitation processes. This study aimed to constrain the mechanisms and thermal window of glauconite alteration, define the progression from smectite authigenesis to illitization, and assess the implications of these transformations on the evolution of porosity and permeability in glauconitic sandstone reservoirs.

2. MATERIALS AND METHODS

2.1. Materials and Hydrothermal Setup. A glauconite-rich greensand sample was collected from the Arnager Greensand Formation along the southern coast of Bornholm Island, Denmark. This Upper Cretaceous succession consists of a quartz-rich, glauconitic sand unit overlain by limestone, reflecting deposition during regional marine transgression [18]. The greensand is characterized by fine-grained, moderately sorted sediment containing abundant glauconite pellets, quartz, minor feldspar, carbonate bioclasts, and fossil fragments, indicating a shallow-marine environment with low sedimentation rates and sustained seawater interaction that promoted glauconite formation [19]. Unconsolidated samples were air-dried, homogenized, and split for baseline petrographic and mineralogical analyses prior to hydrothermal experimentation.

Hydrothermal experiments were designed to simulate burial-related diagenetic conditions and evaluate clay-mineral transformations under controlled fluid–rock interactions. Approximately 20 g of homogenized greensand was placed in a 50-μm stainless-steel mesh pouch and loaded into an Ollital OLT-HP-500 multi-position autoclave system (Figure 1). Each reactor was filled with 200 mL of natural Red Sea water to ensure a high fluid–rock ratio. The vessels were sealed, pressurized with nitrogen, and heated to 80, 150, 200, and 250 °C for 21 days (Table 1), following established experimental protocols [20,21]. During heating, the pressure increased with temperature, and both were monitored throughout the experiments. After each run, the reactors were cooled to room temperature before opening. The solid products were retrieved from the mesh containers, air-dried, and subdivided for petrographic, mineralogical, and geochemical analyses.

2.2. Analytical Methods. A petrographic characterization of the starting material was performed using a polarized-light microscope to determine the framework-grain composition and to assess the abundance and texture of the glauconite pellets. The clay morphology and microtextural features were examined using a scanning electron microscope (SEM) equipped with backscattered electron imaging and energy-dispersive spectroscopy (EDS) for elemental analysis. Samples were mounted on aluminum stubs, coated with a thin conductive layer, and analyzed at accelerating voltages of 10–15 kV. The bulk elemental compositions of the starting and reacted solids were determined using wavelength-dispersive X-ray fluorescence (XRF) following lithium borate fusion. Fused glass beads were prepared from powdered samples (1 g) and analyzed using calibrated reference standards. Measurements were calibrated and quality-controlled using the WROXI-CRM BASED WD certified reference material suite (Malvern Panalytical), certified in accordance with ISO 17034 and ISO Guide 35. Calibration using these matrix-matched fused-bead standards minimized matrix effects and ensured the accuracy and reproducibility of the WD-XRF analyses. Mineralogical analyses of bulk samples and clay fractions (<2 μm) were performed using X-ray diffraction (XRD) with Cu Kα radiation. Bulk powders were scanned over 4-70°2θ range. Clay fractions were separated by dispersion and centrifugation, mounted as oriented aggregates, and analyzed in air-dried, glycolated (70 °C, 20 h), and heated (550 °C, 1 h) states to differentiate expandable and non-expandable phases. Mineral identification and semiquantitative estimates were obtained using standard database matching procedures. Pre- and post-reaction fluids were analyzed for major cations using inductively coupled plasma mass spectrometry (ICP-MS) after appropriate dilution. Prior to ICP-MS analysis, the samples were diluted with 1% ultrapure HNO3. The dilution factor was adjusted according to sample conductivity to achieve a final conductivity below 200 μS/cm, thereby minimizing matrix effects associated with the high salinity of the reacted seawater samples and ensuring reliable elemental determination.

3. RESULTS

3.1. Characterization of the Starting Material. The starting greensand contained moderately sorted quartz and feldspar grains with clay-rich green pellets of glauconite (Figure 2a–b). Bulk geochemical analysis (Table 2) indicated that SiO_2 was the dominant component (80.3 wt%), followed by Al_2O_3 (5.7 wt%), Fe_2O_3 (4.6 wt%), and CaCO3 (4.3 wt%). Minor amounts of K_2O, MgO, and Na_2O were also present (Table 2). Mineralogical data from the bulk XRD analysis (Figure 3) showed that the sediment was primarily composed of quartz (80%) with subordinate potassium feldspar (10%). Muscovite represented the main mica phase (5%), and calcite (5%) accounted for the carbonate fraction (Figure 3). A petrographic examination (Figure 2b) revealed characteristic green glauconite grains within the detrital framework. SEM imaging further confirmed the presence of feldspar grains and carbonate bioclasts (Figure 2c–d).

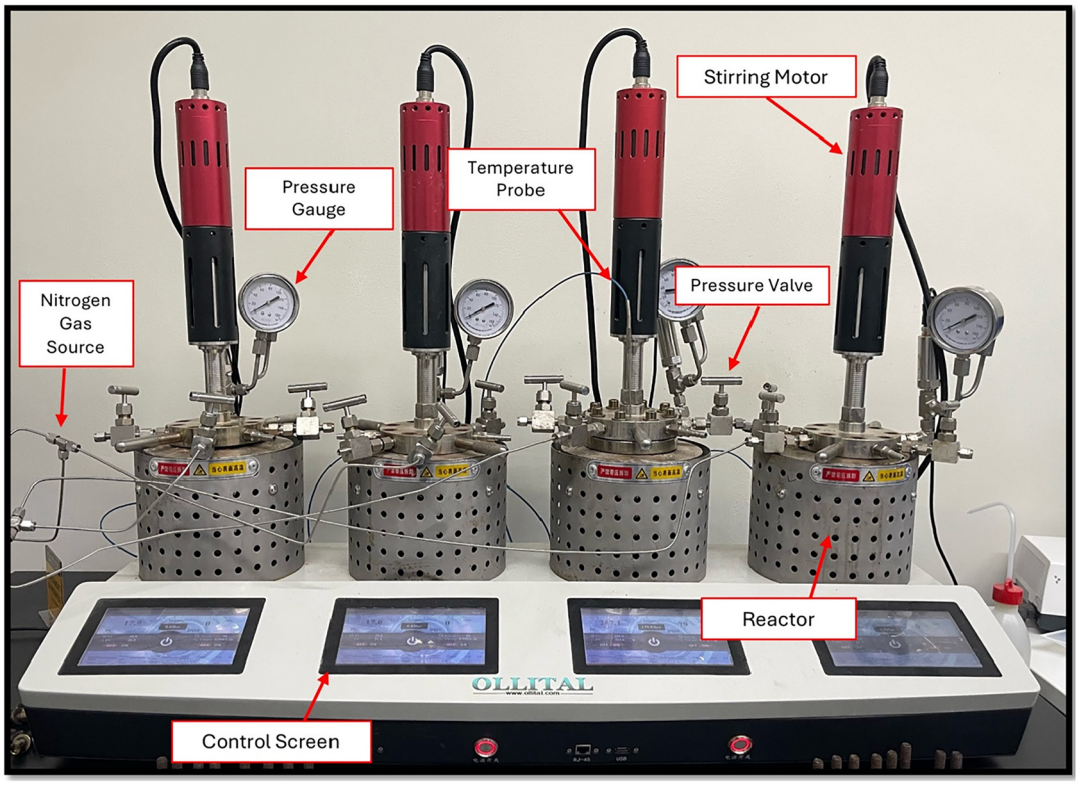


Figure 1. Reactor setup used for the hydrothermal experiments. Each reactor has a capacity of 0.5 L, can be compressed to 160 bars, and heated to 350 °C

3.2. Post-Reaction Mineralogical and Geochemical Evolution. The reacted samples exhibited systematic mineralogical, geochemical, and textural changes as temperature increased, reflecting the progressive diagenetic alteration of the glauconitic greensands. Bulk XRF data (Table 2) indicated that SiO_2 remained the dominant oxide throughout the experiments, consistent with the quartz-rich nature of the starting material. However, significant compositional shifts were observed for other components. The carbonate content decreased significantly, indicating progressive dissolution of calcite (Table 2). K_2O also declined with increasing temperature, whereas Fe_2O_3 increased substantially, reaching 9.1 wt% at 250 °C (Table 2). Minor oxides, including MgO and Na_2O, exhibited consistent enrichment at higher temperatures, suggesting enhanced fluid–rock interactions and redistribution of dissolved species (Table 2). In contrast, Al_2O_3 remained relatively stable, implying limited bulk aluminum loss from the system.

Bulk XRD analysis (Figure 3) confirmed that quartz persisted in approximately 80% of the mineral assemblages throughout the experiments. As in the geochemical analysis, the abundance of calcite and K-feldspar progressively decreased with increasing temperature, reflecting continued dissolution. Clay fraction XRD revealed a clear temperature-dependent transformation pathway (Table 3). At 80 °C, glauconite remained largely detrital, and no significant new clay phases were detected (Table 3). The fluid analyses revealed increased Mg and K concentrations, indicating incongruent dissolution without secondary clay precipitation (Figure 4).

At 150 °C, authigenic smectite first appeared as flakes of grain-coating clay on detrital grains, particularly feldspar (Figure 5). XRD detected expandable clay reflections (Table 3), and SEM imaging revealed fine coatings consistent with Fe-rich smectite (Figure 5a,b). The fluid chemistry at this stage showed enrichment of Fe and a partial decrease in K, suggesting initial K incorporation into the newly formed clays (Figure 4).

Table 2. *XRF results of the samples before and after the experiment (SM, starting material)*

Identification		Major and Minor Elements (wt%)							Trace Elements (ppm)			
Experiment	**Sample ID**	**Al_2O_3**	**K_2O**	**Na_2O**	**Fe_2O_3**	**SiO_2**	**MgO**	**$CaCO_3$**	**SrO**	**P_2O_5**	**TiO_2**	**MnO**
SM	GL@0	5.7	2.9	0.2	4.6	80.3	0.9	4.3	470	1320	4280	180
Exp. 1	GL@80	5.5	2.8	1.1	5.0	79.7	1.1	3.3	220	1360	4230	290
Exp. 2	GL@150	5.8	2.6	1.4	5.6	79.0	2.7	0.7	110	1000	4350	ND
Exp. 3	GL@200	6.1	2.4	1.0	5.8	79.6	2.7	0.6	90	1420	4430	170
Exp. 4	GL@250	5.8	1.7	1.9	9.1	75.7	2.9	0.3	60	280	4170	180

Table 3. *XRD results of clay mineralogy of pre- and post-reaction material*

Sample ID	Normalized Clay Mineralogy (<2 μm) (%)		
	Glauconite	Smectite	Illite
GL@0	99	1	0
GL@80	94	6	0
GL@150	55	43	2
GL@200	21	59	20
GL@250	15	28	57

At 200 °C, glauconite abundance had decreased significantly, and smectite became the dominant mineral in the clay fraction (Table 3). Mixed-layer I/S was first detected at this temperature, marking the onset of illitization. The SEM images display characteristic honeycomb smectite textures alongside the emerging lath-like illite (Figure 6a). Concurrently, an increase in dissolved K indicated rapid dissolution of K-feldspar as temperature increased (Figure 4).

At 250 °C, the clay assemblage was dominated by illite, and the smectite content was substantially reduced. The SEM image shows well-developed fibrous to wavy illite coatings that locally bridge the pore spaces (Figure 7). The fluid compositions at this

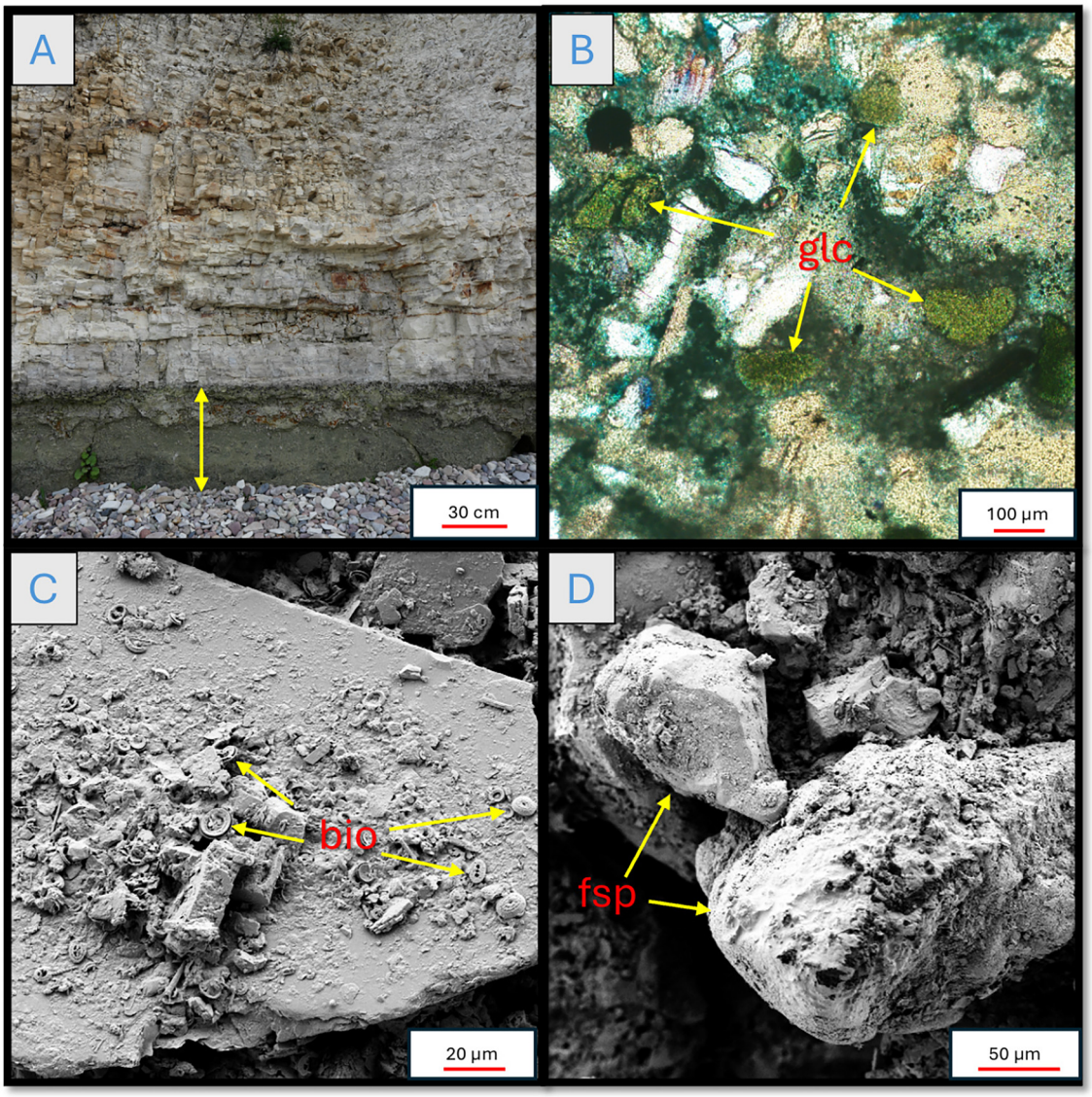


Figure 2. (a) Location of the study area, as indicated by yellow arrow. (b) Thin section of the starting material showing the green glauconite (glc) grains. (c) SEM image showing the bioclast material (bio). (d) SEM showing feldspar (fsp) as detrital grains

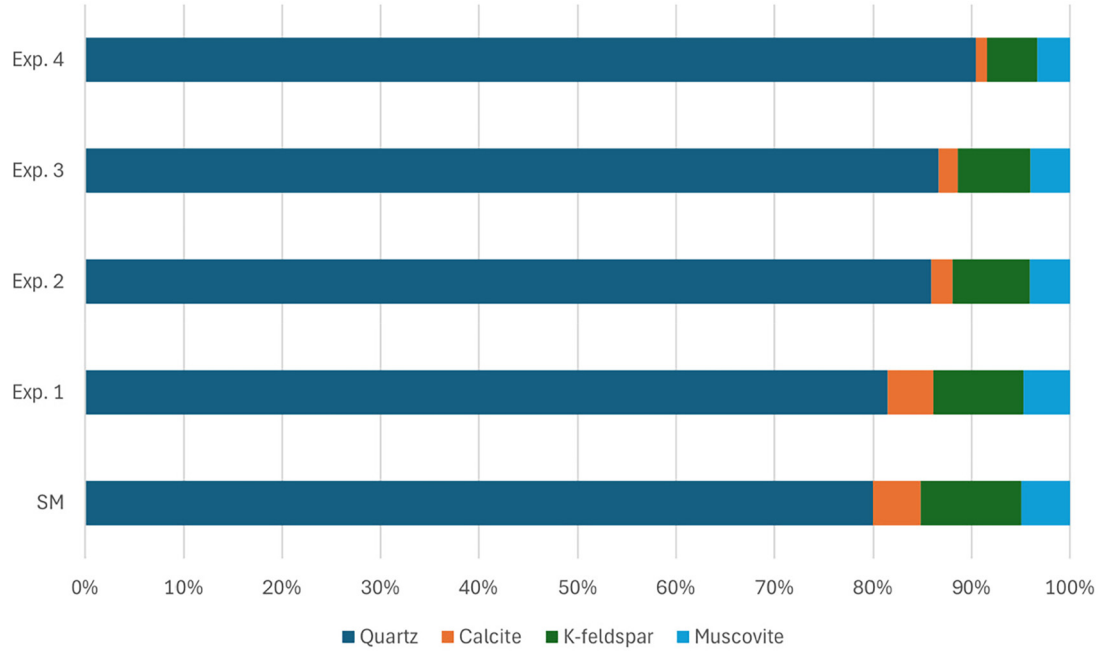


Figure 3. Bulk composition results of pre- and post-experimental material

stage exhibited a significant increase in Fe concentrations, reflecting the continued breakdown of Fe-bearing glauconite (Figure 4). Collectively, the reacted samples displayed a coherent diagenetic progression from glauconite persistence and dissolution at low temperatures, to authigenic smectite formation at intermediate temperatures, and finally to dominant illite under higher thermal conditions, accompanied by distinct changes in clay morphology and bulk composition.

3.3. Textural Evolution of Clay Minerals During Hydrothermal Alteration. Progressive hydrothermal treatment of the glauconitic greensand resulted in systematic textural changes that reflected the transformation from detrital glauconite to authigenic smectite and ultimately to illite. These changes are expressed in the morphology, spatial distribution, and grain–pore relationships of the clay minerals, as observed by SEM. In the starting material, glauconite occurred predominantly as aggregate pellets and composite grains dispersed within

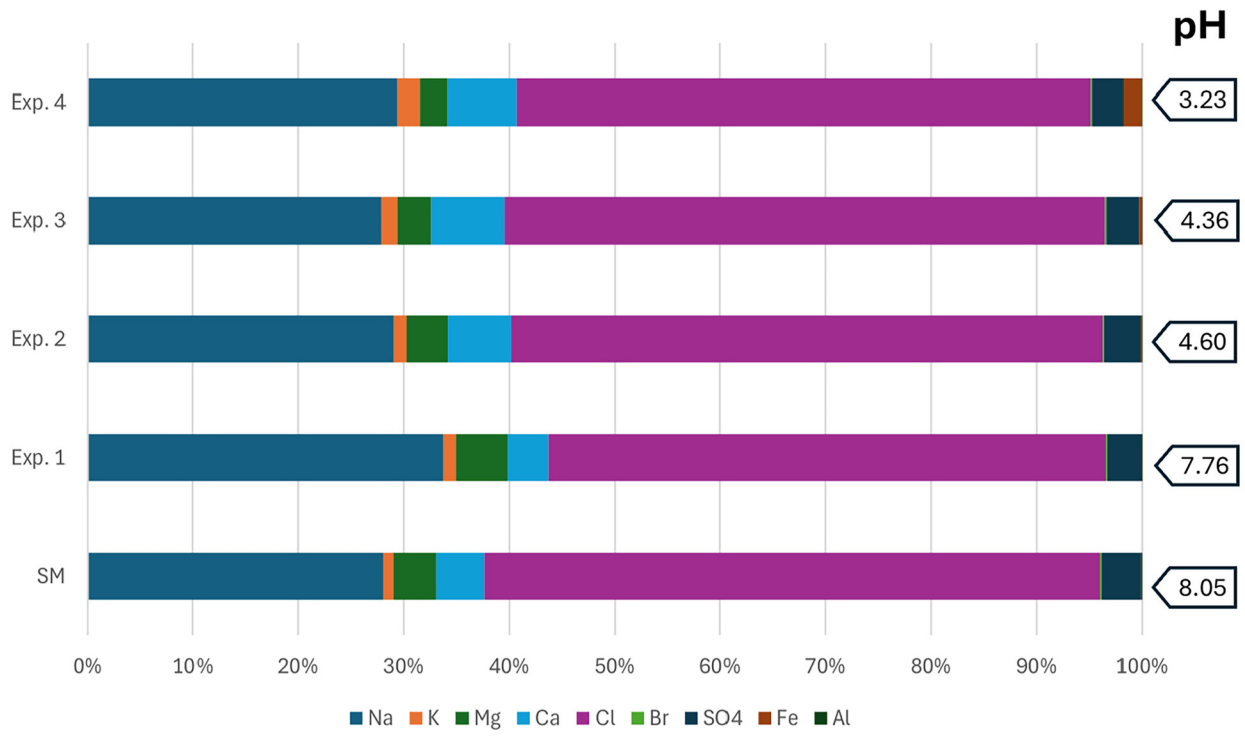


Figure 4. Major and minor ions from ICP-MS analysis, and pH values of the analyzed samples

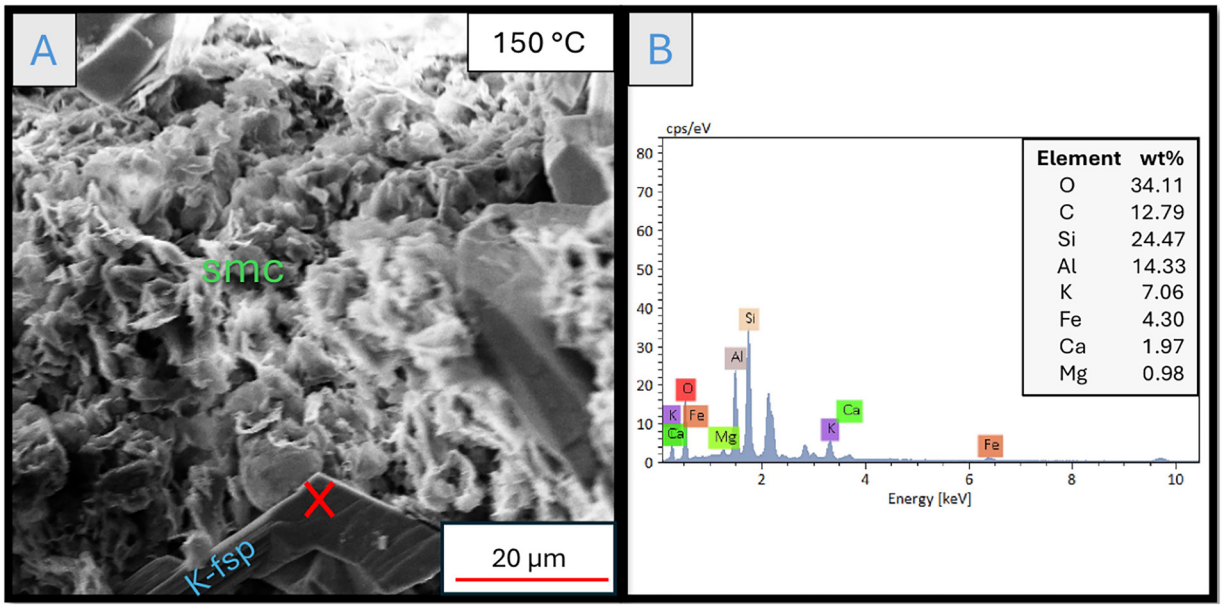


Figure 5. (a) SEM image showing the formation of smectite (smc) as a grain-coating over a detrital grain of K-feldspar (K-fsp). (b) EDS graph representing K-feldspar chemical composition at the red X in (a)

a quartz- and feldspar-dominated framework (Figure 2a–b). The pellets displayed compact internal textures with no evidence of secondary coatings on adjacent detrital grains.

At 80 °C, textural modification was minor. The XRD clay fraction (Table 3) and fluid analysis (Figure 4) indicated glauconite incipient dissolution, but no major clay formation was detected. A marked shift occurred at 150 °C, where authigenic smectite first appeared as thin, discontinuous grain-coating clay (Figure 5). These coatings preferentially developed on the feldspar and quartz surfaces adjacent to the dissolving glauconite. The smectite exhibited flaky-to-platy morphologies and formed micrometer-scale laminar aggregates that partially lined the pore walls (Figure 5a). The distribution was heterogeneous, with thicker coatings near the reactive grain contacts. The pore spaces remained largely open, and clay development occurred primarily through pore lining rather than pore filling.

At 200 °C, smectite became more abundant and texturally mature (Figure 6). The clay displayed characteristic honeycomb and web-like aggregates (Figure 6a) that formed continuous coatings around the detrital grains. Mixed-layer I/S textures began to appear, represented by the coexistence of platy smectite and nascent lath-like illite crystals. The coatings became thicker and locally extended into the pore throats, indicating a transition from simple pore-lining to partial pore-bridging

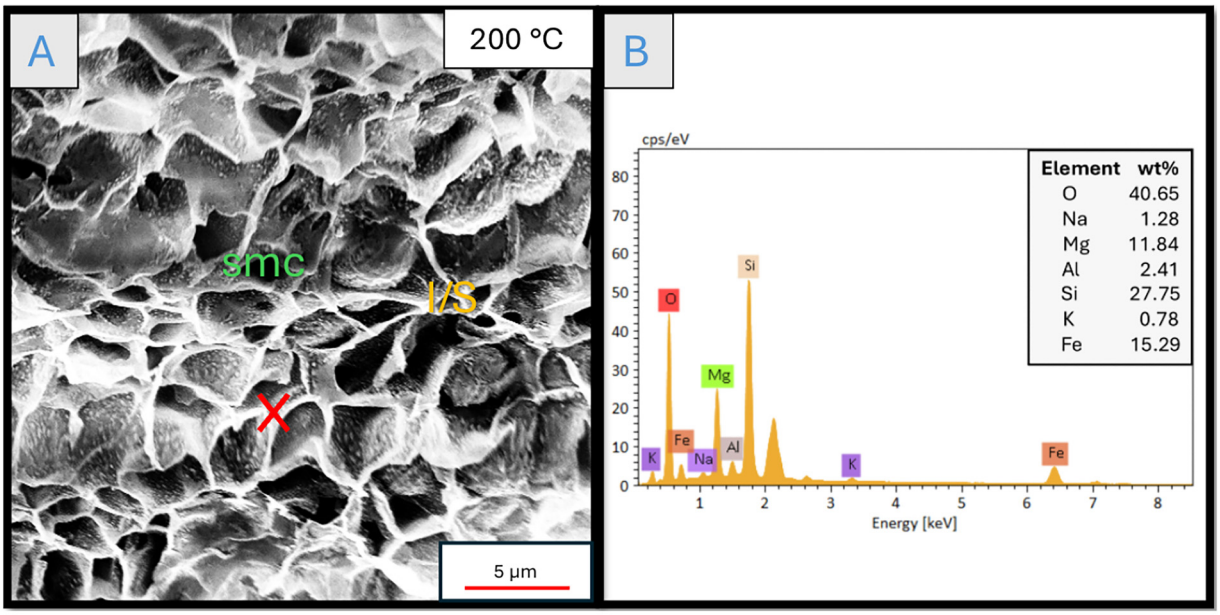


Figure 6. (a) SEM image showing the honeycomb structure of smectite (smc) and formation of the illite/smectite (I/S) mixed layer. (b) EDS graph showing the smectite chemical composition of the red X in (a)

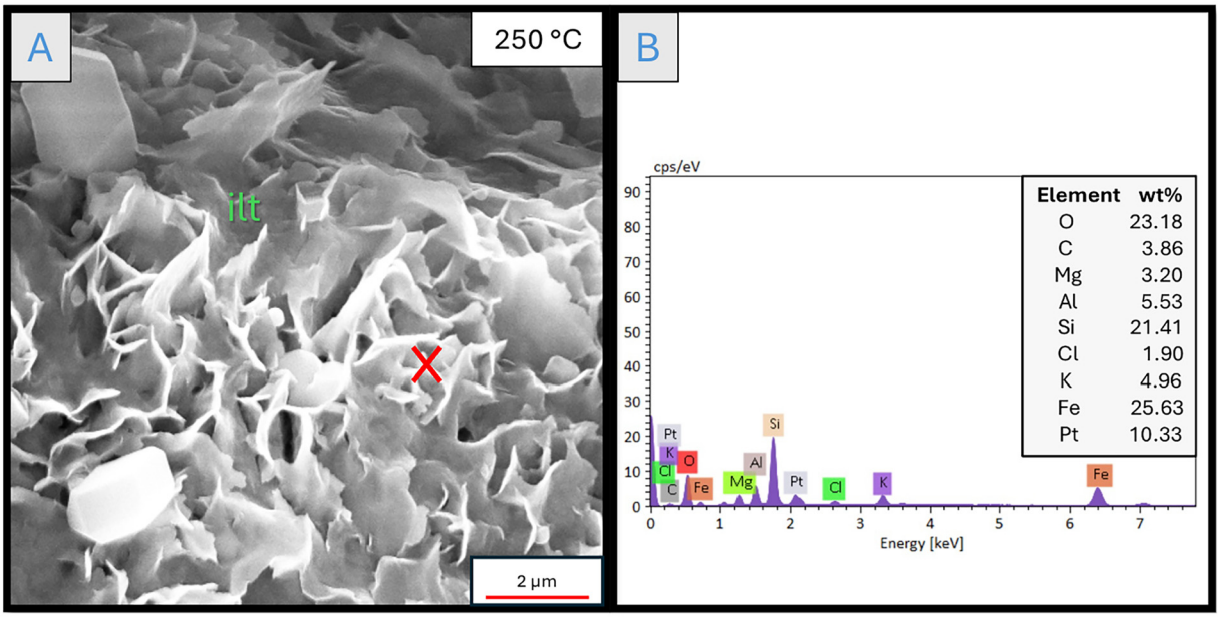


Figure 7. (a) SEM image showing the wavy morphology of the formed illite (ilt). (b) EDS graph illustrating the chemical composition of formed illite at the red X in (a)

morphologies. At 250 °C, the clay assemblage was dominated by well-developed illite with fibrous to wavy morphologies (Figure 7a). Illite occurred as dense aggregates and filamentous networks that coat the grains and frequently bridge the pore throats. Unlike earlier platy smectite coatings, fibrous illite formed interlocking crystal bundles that partially occluded the pore spaces (Figure 7a).

4. DISCUSSION

4.1. Alteration of Labile Minerals and Authigenic Development of Smectite. The experimental results demonstrate that glauconite and its associated labile detrital phases are metastable under burial-relevant hydrothermal conditions and act as the primary sources of dissolved constituents for secondary clay formation. At 80 °C, the observed mineralogical changes were limited, but fluid chemistry indicated incongruent dissolution of glauconite, K-feldspar, and carbonate phases (Figure 3), as reflected by increased concentrations of Mg and K in solution (Figure 4). These trends suggest that the early-stage reactions are dominated by mineral breakdown rather than by the precipitation of new clay phases.

At 150 °C, the development of authigenic smectite as grain-coating clay (Figure 5a) marked the onset of significant secondary mineral growth. The preferential nucleation of the thin flake-like coatings on the feldspar and quartz surfaces indicated heterogeneous nucleation driven by local supersaturation conditions. The formation of smectite at this stage is consistent with temperature-dependent dissolution–precipitation reactions, in which Fe, Mg, and Al are released from glauconite, and framework minerals recombine to form expandable clay phases[12,13,17,22]. The decrease in glauconite abundance with increasing temperature, coupled with the appearance of smectite in the clay fraction XRD data (Table 3), confirms that glauconite alteration represents a key precursor pathway for smectite authigenesis in glauconitic sandstones.

The progressive reduction in calcite and K-feldspar with increasing temperature further supports a fluid-mediated alteration system (Figure 3). These minerals contribute additional Ca, K, and Al to the reacting fluid, thereby facilitating clay nucleation and growth. Overall, the data indicate that smectite formation results from the coupled dissolution of glauconite and detrital grains, followed by the precipitation of Fe–Mg-rich clay coatings under intermediate thermal conditions.

4.2. Mechanisms and Controls on Smectite-to-Illite Transformation. The subsequent transformation of smectite to illite occurred through a mixed-layer I/S intermediate stage (Figure 6a), consistent with established burial diagenetic models[13,23]. Illitization became evident at 200 °C, and at 250 °C, illite dominated the clay assemblage, displaying fibrous to wavy morphologies (Figure 7A) characteristic of advanced diagenesis.

Two principal factors govern this transformation. First, the temperature and duration of thermal exposure strongly influence the reaction progress. The proportion of illite increased systematically with increasing temperature, demonstrating that the conversion was kinetically driven[24]. Second, K availability plays a critical role[25]. As temperature increases, potassium released by dissolving K-feldspar and mica is incorporated into the interlayer spaces of smectite. This K fixation increases the layer charge and causes the expandable layers to collapse, gradually stabilizing a non-expandable 10 Å structure typical of illite. At intermediate temperatures, this process produces mixed-layer I/S, indicating partial conversion. With further heating, continued potassium uptake and temperature-driven ordering lead to a greater proportion of illite layers, resulting in predominant illite at the highest temperature. The overall transformation proceeds through a combination of dissolution-reprecipitation and structural reorganization mechanisms, as indicated by the changes in clay morphology and fluid chemistry. Together, these processes explain the progressive conversion of smectite-rich coatings into illite-dominated assemblages as temperature increases.

The observed increase in aqueous K at 200 and 250 °C (Figure 4), along with declining K-feldspar content (Figure 3), indicates that K was mobilized from detrital feldspar and incorporated into growing illite. However, bulk-rock K2O trends alone do not fully capture the reaction progress, as simultaneous dissolution and redistribution of K between solids and fluids can obscure whole-rock compositional signals. Therefore, mineralogical evidence from XRD and SEM provides the most reliable indication of illitization.

Smectite derived from glauconite is relatively enriched in Fe and Mg, which may have delayed complete illitization at intermediate temperatures. Such compositional factors influence the reaction rates and structural reorganization[12]. The progression from flaky smectite coatings to fibrous illite suggests a combination of layer reordering and dissolution–reprecipitation processes during the transformation. The final assemblage at 250 °C reflects advanced illitization driven by elevated temperatures and sufficient K supply.

4.3. Reservoir Quality Implications. This evolution of clay minerals has direct implications for the reservoir performance of glauconitic sandstones. At intermediate temperatures, smectite and mixed-layer I/S form as grain coatings (Figure 6a). Such coatings are widely recognized for their capacity to inhibit quartz overgrowth by reducing the reactive grain surface area, thereby preserving the primary porosity[26]. In this context, early-stage glauconite alteration may contribute to porosity retention by forming protective clay films that limit silica cementation.

In contrast, the development of fibrous illite at higher temperatures (Figure 7a) leads to distinct reservoir outcomes. SEM images show that illite forms pore-lining and local pore-bridging networks, significantly reducing permeability by constricting pore throats and increasing flow-path tortuosity[27]. Although the total pore volume may remain partially preserved owing to the inhibited quartz cementation, the effective permeability may decline sharply once fibrous illite becomes dominant.

The presence of expandable smectite layers during the intermediate stages also introduces potential water-sensitivity risks. Mixed-layer I/S containing significant smectite components may contribute to swelling or migration of fine grains under changing fluid conditions. Consequently, glauconitic sandstones may experience a dual diagenetic effect in which early clay development promotes porosity preservation, whereas later illitization reduces permeability. Therefore, the net reservoir quality depends on the balance between quartz-cement inhibition and pore-throat obstruction by authigenic clays.

4.4. Limitations and Future Work. The hydrothermal experiments were conducted for a fixed duration, which accelerated natural burial processes and may not fully replicate long-term kinetic pathways. Natural systems operate over geological timescales and may involve variable fluid fluxes, pressure regimes, and redox conditions that influence reaction mechanisms. Additionally, the mechanical compaction effects and evolving stress conditions, which strongly influence the evolution of natural reservoirs, were not incorporated into the experimental design.

Future research should explore longer-duration experiments, variable fluid compositions, and controlled redox environments to more accurately simulate basin conditions. Reactive transport modeling can improve the quantitative predictions of clay mineral evolution. Finally, pore-scale imaging and permeability measurements would allow the direct evaluation of petrophysical changes associated with progressive illitization in glauconitic reservoirs.

5. CONCLUSIONS

This study investigated the diagenetic alteration of glauconitic greensand under burial-relevant hydrothermal conditions to constrain the pathway from glauconite to smectite, and ultimately to illite, and to evaluate the implications for reservoir quality evolution. The results demonstrated a systematic, temperature-dependent transformation sequence controlled by coupled dissolution–precipitation reactions and K availability. Our major findings are as follows:

- At low temperatures (80 °C), the dissolution of glauconite and detrital phases enriched the fluid in Mg and K without significant authigenic clay formation. At 150 °C, authigenic smectite developed as a grain coating. At 200 °C, mixed-layer I/S formed, indicating incipient illitization facilitated by K fixation. By 250 °C, illite had become the dominant clay phase and exhibited fibrous morphologies.
- These mineralogical and textural changes have direct implications for reservoirs. The grain-coating smectite and mixed-layer I/S formed during the intermediate stages may inhibit quartz cementation and preserve porosity. In contrast, the fibrous and pore-bridging illite formed at higher temperatures can significantly reduce the permeability by constricting the pore throats.

Consequently, glauconitic sandstone reservoirs may experience a diagenetic scenario in which porosity is retained while permeability declines. In summary, the overall quality of such reservoirs is governed by the morphology and distribution of clay.

AFFILIATIONS AND AUTHOR DETAILS

Undergraduate Author

Fatimah Al Ibrahim – *Department of Geoscience, College of Petroleum Engineering and Geosciences, King Fahd University of Petroleum & Minerals, Dhahran 31261, Kingdom of Saudi Arabia*; 0009-0008-6637-1310
Email: s202467960@kfupm.edu.sa

Corresponding Author

Anas Muhammad Salisu – *Research Mentor, Research Scientist, Center for Integrative Petroleum Research, College of Petroleum Engineering and Geosciences, King Fahd University of Petroleum & Minerals, Dhahran, Saudi Arabia*; 0009-0002-6134-0511
Email: anas.salisu@kfupm.edu.sa

ACKNOWLEDGEMENTS

The authors gratefully acknowledge the Department of Geosciences and College of Petroleum Engineering and Geosciences

(CPG) at King Fahd University of Petroleum and Minerals (KFUPM) for providing the laboratory facilities and technical support essential for this study. We extend our deep appreciation to Prof. Khalid Al-Ramadan for his continuous support, guidance, and encouragement throughout this study. We also thank Dr. Ayman Al-Lehyani for his valuable support during this study. Special thanks are given to Fatima Al-Shammary, Ayah Alaradi, Ayah Alkhalifah, and Shahad Darwish for their assistance with fieldwork and sample collection in Denmark. We also acknowledge the Arabian Drilling Company for supporting our field visit to Bornholm, which enabled sample collection and geological evaluations.

REFERENCES

(1) Fernández-Landero, S. & Fernández-Caliani, J. C. Mineralogical and Crystal-Chemical Constraints on the Glauconite-Forming Process in Neogene Sediments of the Lower Guadalquivir Basin (SW Spain). *Minerals 2021, Vol. 11, Page 578* **11**, 578 (2021).

(2) Hegab, O. A. & Abd El-Wahed, A. G. Origin of the glauconite from the Middle Eocene, Qarara Formation, Egypt. *Journal of African Earth Sciences* **123**, 21–28 (2016).

(3) Diaz, E., Prasad, M., Mavko, G. & Dvorkin, J. Effect of glauconite on the elastic properties, porosity, and permeability of reservoir rocks. *The Leading Edge* **22**, 42–45 (2003).

(4) Zhang, Q. & Tutolo, B. M. Geochemical evaluation of glauconite carbonation during sedimentary diagenesis. *Geochim. Cosmochim. Acta* **306**, 226–244 (2021).

(5) Bansal, U., Banerjee, S., Ruidas, D. K. & Pande, K. Origin and geochemical characterization of the glauconites in the Upper Cretaceous Lameta Formation, Narmada Basin, central India. *Journal of Palaeogeography* **7**, 99–116 (2018).

(6) Weibel, R. *et al.* Reactivity of glauconitic sandstones in CO2 experiments. *International Journal of Greenhouse Gas Control* **148**, (2025).

(7) Worden, R. & Morad, S. Clay Minerals in Sandstones: Controls on Formation, Distribution and Evolution. in *Clay Mineral Cements in Sandstones* vol. 34 1–41 (2009).

(8) Walderhaug, O. & Porten, K. W. How Do Grain Coats Prevent Formation of Quartz Overgrowths? *Journal of Sedimentary Research* **92**, 988–1002 (2022).

(9) Ajdukiewicz, J. M. & Larese, R. E. How clay grain coats inhibit quartz cement and preserve porosity in deeply buried sandstones: Observations and experiments. *Am. Assoc. Pet. Geol. Bull.* **96**, 2091–2119 (2012).

(10) Bloch, S., Lander, R. H. & Bonnell, L. Anomalously High Porosity and Permeability in Deeply Buried Sandstone Reservoirs: Origin and Predictability. *Am. Assoc. Pet. Geol. Bull.* **86**, 301–328 (2002).

(11) Griffiths, J. *et al.* Origin and distribution of grain-coating and pore-filling chlorite in deltaic sandstones for reservoir quality assessment. *Mar. Pet. Geol.* **134**, (2021).

(12) Baldermann, A. *et al.* The role of Fe on the formation and diagenesis of interstratified glauconite-smectite and illite-smectite: A case study of Lower Cretaceous shallow-water carbonates. *Chem. Geol.* **453**, 21–34 (2017).

(13) Lanson, B., Sakharov, B., Claret, F. & Drits, V. Diagenetic Smectite-to-Illite Transition in Clay-Rich Sediments: A Reappraisal of X-Ray Diffraction Results Using the Multi-Specimen Method. *Am. J. Sci.* **309**, 476–516 (2009).

(14) Peretyazhko, T. S. *et al.* Smectite formation in the presence of sulfuric acid: Implications for acidic smectite formation on early Mars. *Geochim. Cosmochim. Acta* **220**, 248–260 (2018).

(15) Roberson, H. E. & Lahann, R. W. Smectite to Illite Conversion Rates: Effects of Solution Chemistry. *Clays Clay Miner.* **29**, 129–135 (1981).

(16) Lahann, R. W. Smectite diagenesis and sandstone cement: the effect of reaction temperature. *J. Sediment. Petrol.* **50**, 755–760 (1980).

(17) Al-Ramadan, K. Illitization of Smectite in Sandstones: The Permian Unayzah Reservoir, Saudi Arabia. *Arab. J. Sci. Eng.* **39**, 407–412 (2014).

(18) Hart, M. B., Bromley, R. G. & Packer, S. R. Anatomy of the stratigraphical boundary between the Arnager Greensand and Arnager Limestone (Upper Cretaceous) on Bornholm, Denmark. *Proceedings of the Geologists' Association* **123**, 471–478 (2012).

(19) Schack Pedersen, S. A. & Gravesen, P. The geological framework for Hvideklint, south-east Denmark, using glaciodynamic sequence stratigraphy. *GEUS Bulletin* **47**, (2021).

(20) Bello, A. M., Salisu, A. M. & Amao, Abduljamiu Olalekan, Umar, Mustapha, Al Ramadan, K. Experimental development of chlorite: insights from a kaolinite precursor. *Journal of Sedimentary Research* **95**, 1–24 (2025).

(21) Salisu, A. M., Bello, A. M., Amao, A. O., Lander, R. H. & Al-Ramadan, K. experimental study of smectite authigenesis and its subsequent illitization: insights from modern estuary sediments. *Journal of Sedimentary Research* https://doi.org/10.2110/jsr.2024.135 (2025) doi:10.2110/jsr.2024.135.

(22) Small, J. S. Fluid composition, mineralogy and morphological changes associated with the smectite-to-illite reaction: An experimental investigation of the effect of organic acid anions. *Clay Miner.* **29**, 539–554 (1994).

(23) Inoue, A., Kohyama, N., Kitagawa, R. & Watanabe, T. Chemical and Morphological Evidence for the Conversion of Smectite to Illite. *Clays and Clay Minerals - Clays Clay Miner* **35**, 111–120 (1987).

(24) Pytte, A. M. & Reynolds, R. C. The thermal transformation of smectite to illite. in *Thermal history of sedimentary basins: Methods and case histories* 133–140 (Springer, 1989).

(25) Hellmann, R. *et al.* The hydrothermal alkaline alteration of potassium feldspar: A nanometer-scale investigation of the orthoclase interface. *Chem. Geol.* **569**, 120133 (2021).

(26) Tang, L., Gluyas, J. & Jones, S. Porosity preservation due to grain coating illite/smectite: Evidence from Buchan Formation (Upper Devonian) of the Ardmore Field, UK North Sea. *Proceedings of the Geologists' Association* **129**, 202–214 (2018).

(27) Wilkinson, M., Haszeldine, R. S., Fallick, A. E. & Shaw, H. Authigenic illite within northern and central North Sea oilfield sandstones: evidence for post-growth alteration. *Clay Miner.* **49**, 229–246 (2014).